Available online at www.sciencedirect.com

ScienceDirect

Procedia Engineering 10 (2011) 1479–1484

Engineering Procedia

ICM11

Observation of Fatigue Crack Propagation Behavior under Torsional Loading by Using Synchrotron Radiation Micro-CT Imaging

Daiki Shiozawa[a]*, Yoshikazu Nakai[a], Tomonori Murakami[a], and Hiroaki Nosho[a]

a Graduate School of Engineering, Kobe University, 1-1 Rokkodai, Nada-ku, Kobe, 657-8501, Japan

Abstract

In the present study, synchrotron radiation micro computed tomography (SR μCT) imaging of SPring-8 was applied to the observation of the torsion fatigue crack propagation behavior. The transition of crack propagation from Mode II to I occurs under torsion fatigue. The conventional technique, such as optical microscope and scanning microscope, cannot give us the crack growth behavior under the surface. Therefore, the transition of crack propagation could not be discussed in detail. The compact torsion fatigue-testing machine was developed for fatigue testing at SPring-8, and the torsion fatigue tests and measurements of SR micro-CT were carried out alternately. The shape of torsion fatigue cracks could be evaluated quantitatively and nondestructively. Transition of crack propagation from Mode II to Mode I under the surface could be observed. The condition of transition of crack propagation was discussed by using three-dimensional shape of cracks.

Keyword: Micro Computed Tomography Imaging, Synchrotron Radiation, Torsion fatigue, Crack Propagation Behavior, Ti-6Al-4V;

1. Introduction

Recently the behavior of fatigue cracks under mixed mode loading has been studied by several researchers [1],[2]. The crack propagation behavior under torsion fatigue is complex, such as the transition of crack propagation from Mode II to I. The crack propagation behavior during fatigue is usually studied through the observation of cracks on the surface with direct or indirect method. However, it is not easy to evaluate the behavior of cracks, simply by the conventional technique, such as the replication technique. It give us only the information at the surface. Therefore, the transition condition of crack propagation could not be discussed in detail. The micro computed tomography (μCT) with synchrotron radiation could make possible to monitor the shape of cracks inside the material continuously or intermittently.

The authors have been applied μCT with synchrotron radiation of SPring-8 to the three-dimensional measurement of inclusion and cracks in steels and fretting fatigue cracks [3]-[6]. In the present study, the behavior of fatigue cracks from the initiation to the fracture was observed and the condition of transition of crack propagation

* Corresponding author. Tel.: +81-78-803-6329; fax: +81-78-803-6155.

1877-7058 © 2011 Publi d by Elsevier Ltd. Open access under CC BY-NC-ND license.
doi:10.1016/j.proeng.2011.04.247

mode was discussed by using three-dimensional shape of cracks. A compact torsion fatigue testing machine was developed to facilitate the experiments at SPring-8.

2. Experimental procedure

2.1. Torsion fatigue-testing machine

It is convenient that a fatigue-testing machine can be set on a sample stage in an experimental hatch of a beam-line for observation of fatigue propagation behavior. It is not feasible to evaluate microscopic fatigue propagation behavior of specimens of a standard size, because of the overweight of the machine for the sample stage. A compact fatigue-testing machine, which can be set nearby the experimental hatch, is developed.

The newly developed torsion fatigue-testing machine is shown in Fig. 1. The dimension and mass of the machine are approximately 500mm × 200mm × 200mm, and 10kg respectively. The machine is transportable and can be placed on a desk. The torque is applied by a direct drive motor. The capacity of the motor is 5.0Nm. The rotary type motor directly transfers the torque to the specimen, so that the fatigue-testing machine does not require load transfer mechanism, then downsizing of machine and greater precision torque control are possible. In this experiments, fully reversed cyclic torsion load (R= −1) with a frequency of 10 Hz was applied to the specimen.

2.2. Material and specimen

The material for this study was a titanium alloy, (JIS Ti-6Al-4V). The chemical composition of this titanium alloy is as follows: 0.01C, 3.96V, 6.23Al, 0.14O, 0.01N, 0.15Fe, and balance Ti (in mass%). The 0.2% proof stress is 868 MPa, the tensile strength was 995 MPa, and the elongation is 18%. The shape and dimensions of the specimen are shown in Fig. 2. Figure. 3 shows the microstructures of Ti-6Al-4V used in the present study. The microstructures is equiaxial and the average grain size is 8μm.

2.3. Measurement method

X-ray imaging was carried out at BL19B2 beam line of SPring-8, which is the large synchrotron radiation facility in Japan. X-ray energy was adjusted to 35keV with silicon double-crystal monochromator. The distance between a bending magnet (X-ray source) and the specimen was about 100m. The projection image of penetrated X-ray was observed by an X-ray area detector. The detector was composed of a beam monitor (Hamamatsu Photonics AA50) and cooled CCD camera (Hamamatsu Photonics C4880 41S). Transmitted X-ray is converted to visible light

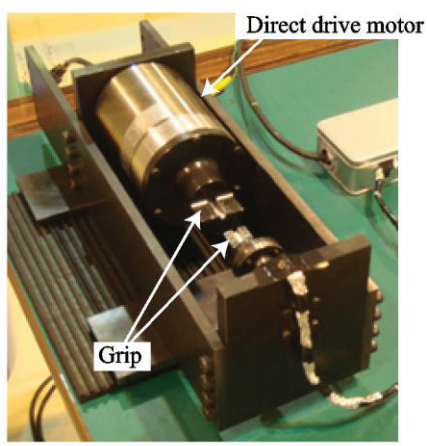

Fig. 1 Newly-developed torsion fatigue testing machine

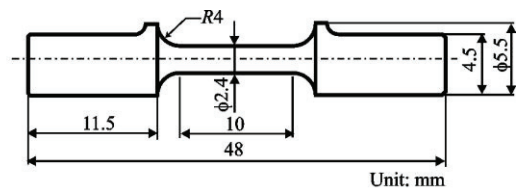

Fig. 2 Shape of specimen.

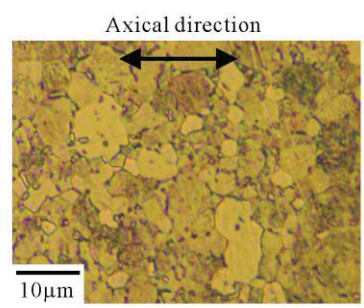

Fig. 3 Optical microscope of metallographic structure

through a thin phosphor screen and projected to the CCD camera by an optical relay-lens. Series of projection images of the specimen were obtained every 0.3° from 0° to 180° by rotating the specimen. To utilize the phase contrast effect, the X-ray area detector was set by 0.7m behind the sample. Slice images were reconstructed from the series of projection images by filtered-back projection algorithm. It provides a 3D image with a greyscale color map that is proportional to the local X-ray attenuation coefficient.

3. Experimental results and discussion

Figure 4 shows the CT images of the crack (Crack A) under τ_a=450 MPa. These images indicate the map of X-ray attenuation coefficient. Cracks are obtained as black line or, white and black lines due to the phase contrast. The phase contrast effect generates distinct white and black lines at the interface of structures. So that the phase contrast emphasizes the crack where crack opening distance is small. The propagation behavior can be observed intermittently by using the newly fatigue-testing machine and SR μCT imaging. The torsion crack initiated and propagated in the direction parallel to the specimen axis by the sliding mode. At N=1.84×10^{5}cycles, crack branched under surface, as shown in Fig. 4(c).

In the tomographic images, the position of the crack tip can be determined via simple visual inspection using image-editing software when the contrast of crack image is high. Otherwise, it should be determined manually. Plug-in for the software of Image J allows for retrieving the coordinates of the pixel that is manually selected as the crack tip at each slice through the sample thickness. Figure 5 shows shapes and dimensions of torsion cracks obtained from the μCT images. Closed circles indicate the crack tips before branching, and open circles indicate the branched crack tips. The crack growth in the depth direction can be identified from 1.53×10^5 cycles to 1.64×10^5 cycles. The growth of the branched crack started after the crack depth increased up to the 320μm. And then, the branched crack length increased with increasing in number of cycles, and the crack resumed the propagation in the

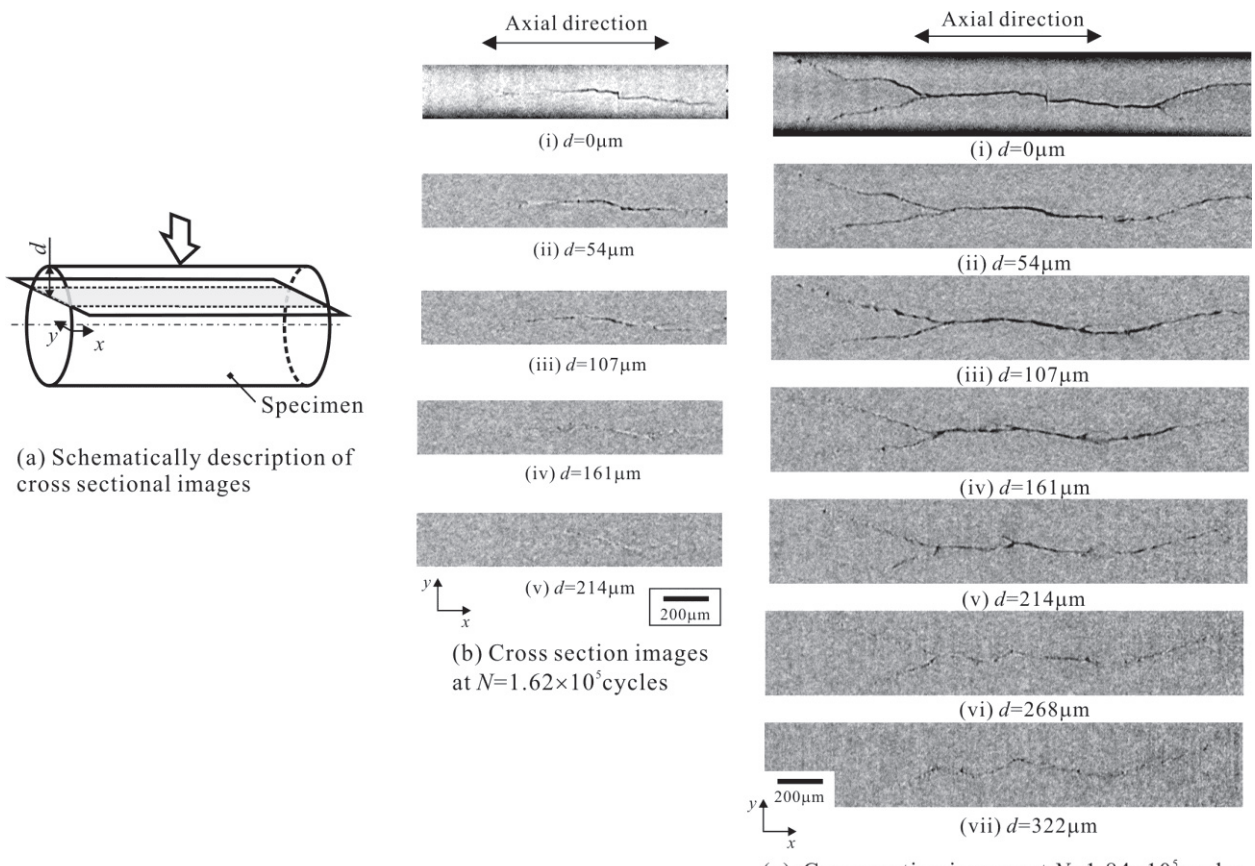

Fig. 4 CT image of Crack A under τ_a=450MPa

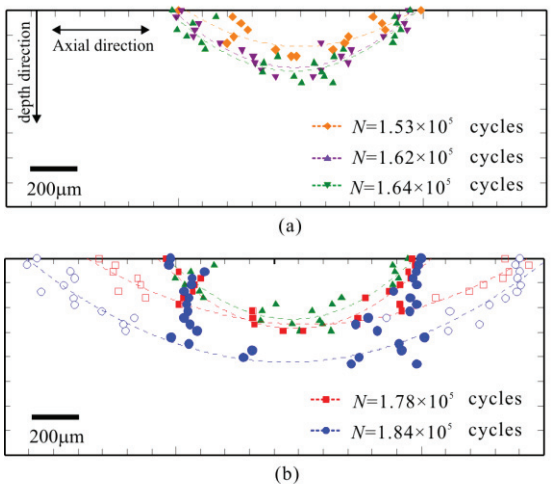

Fig. 5 Internal shape of Crack A by measured by slices of μCT images.

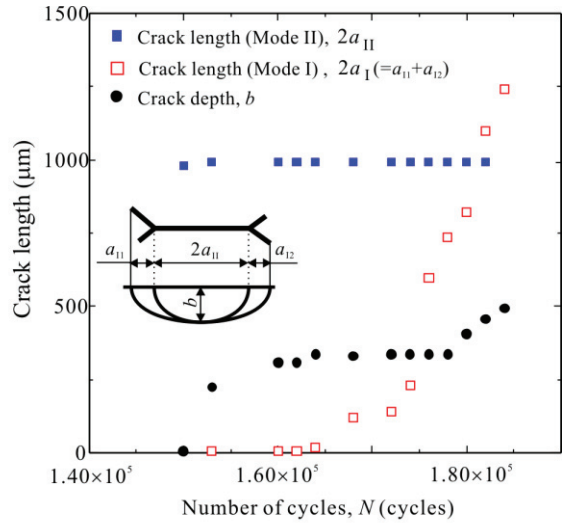

Fig. 6 Crack growth curves of Crack A.

depth direction.

Figure 6 shows crack growth curve of Crack A. The crack lengths on the surface was observed by the optical microscope and CT imaging, and crack depth was measured by μCT image. The torsion crack was detected on the surface by optical microscope at N=9.30×10^4 cycles. On the other hand, the crack could not be detected by the μCT image until N=1.53×10^{5}cycles. It is considered that the crack is not enough scale to be detected by the detector from N=9.30×10^4 to 1.50×10^{5}cycles. The crack depth increased with increasing in the number of cycles from N=1.53×10^5 to 1.60×10^{5}cycles, though the crack rarely propagated at the surface. The non-propagation of Mode II crack is related to the crack tip shielding [7],[8].

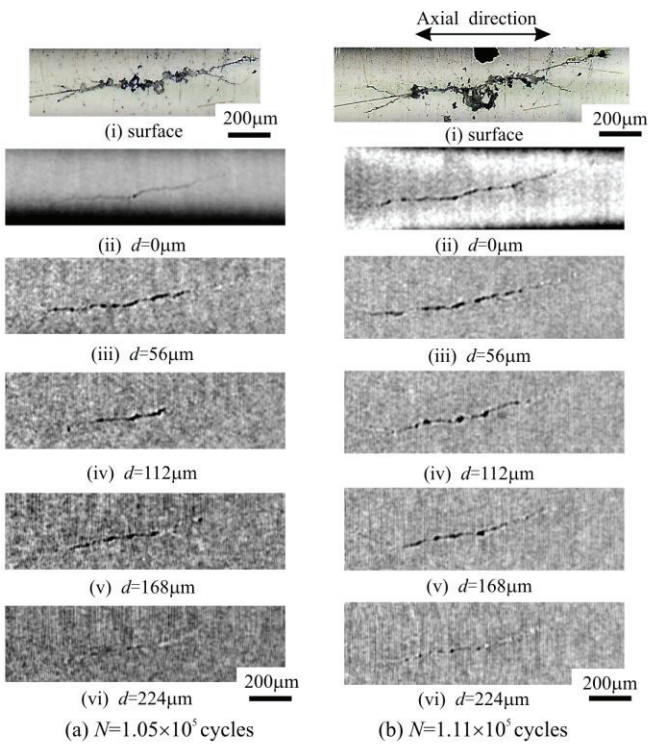

Fig. 7 CT image of Crack B under τ_a=435MPa, (i) is obtained by optical microscope, (ii)~(vi) are obtained by CT

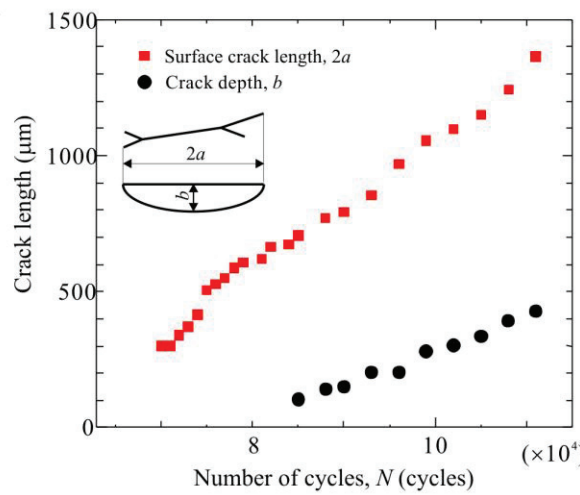

Fig. 8 Crack growth curve of Crack B

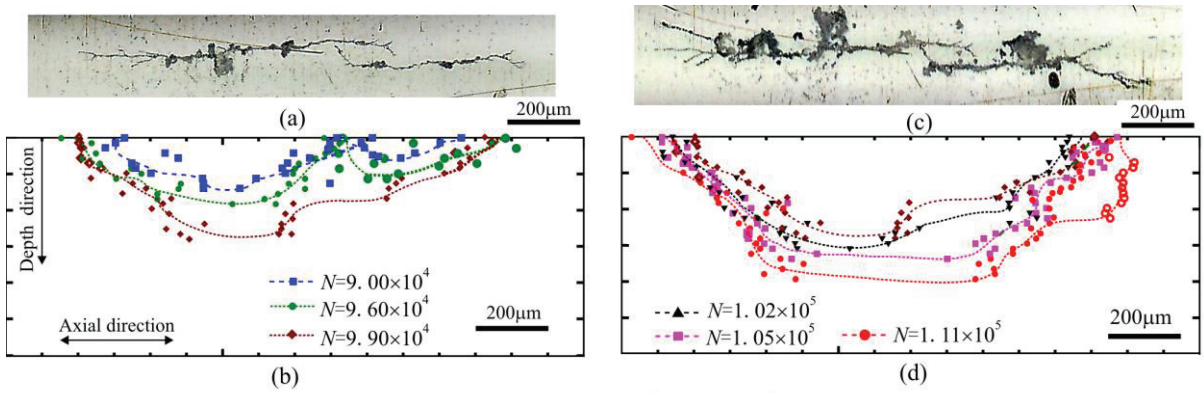

Fig. 9 Crack propagation behavior of Crack C from N=9.00×10^4 to 1.11×10^5 cycles, (a) : Optical micrograph at N=9.90×10^{4}cycles, (c) : Optical micrograph at N=1.11×10^{5}cycles, (b) and (c) : Internal crack shape obtained by CT.

The CT images of the crack (Crack B) under τ_a=435 MPa are shown in Fig. 7. It is found from Fig. 7 that the branching of crack could not be observed under the surface at N=1.05×10^5 and 1.11×10^5 cycles. It is considered that the crack propagation mode has not changed from the sliding mode to the opening mode. Figure 8 shows the crack growth curve of Crack B. From N=7.2 ×10^4 to 8.5×10^4 cycles, the crack had been observed on the surface by the optical microscope, but the crack could not be detected by the CT imaging, like Crack A. The crack depth and crack length on the surface increased with increasing in the number of cycles. The crack depth had been detected since the abrasion powders were observed on the cracks at the surface, as shown in Fig. 7.

The optical micrographs and internal shape of the crack (Crack C) under τ_a=435 MPa are shown in Fig. 9. In Fig. 9, open circles indicate the branched crack tips. Two cracks coalesced to Crack C at N=9.90×10^4 cycles. The crack growth rate in the depth direction increased just before and after the crack coalescence, compared with that in the axial direction, and then the one large crack was formed. After the crack coalescence, the crack branching was observed both on and under the surface. The crack branching is considered to be due to the crack coalescence for Crack C.

The stress intensity factor ranges, ΔK_{I}, ΔK_{II}, and ΔK_{III}, are evaluated, and plotted against the number of cycles in Fig. 10, where $\Delta K_{\mathrm{I(A)}}$ and ΔK_{II} are the stress intensity factors at the crack tip at the surface, and $\Delta K_{\mathrm{I(B)}}$ and ΔK_{III} are the stress intensity factors at the depth of crack tip. The stress intensity factor range, ΔK_{II} and ΔK_{III} were calculated by using Kaissir and Sih's equation [9] based on the crack shape projected to the plane parallel to the specimen axis,

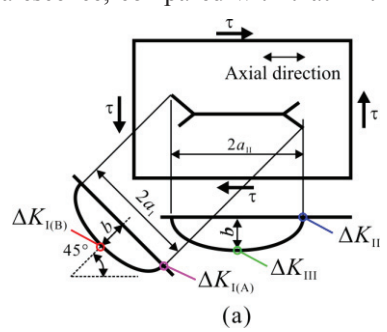

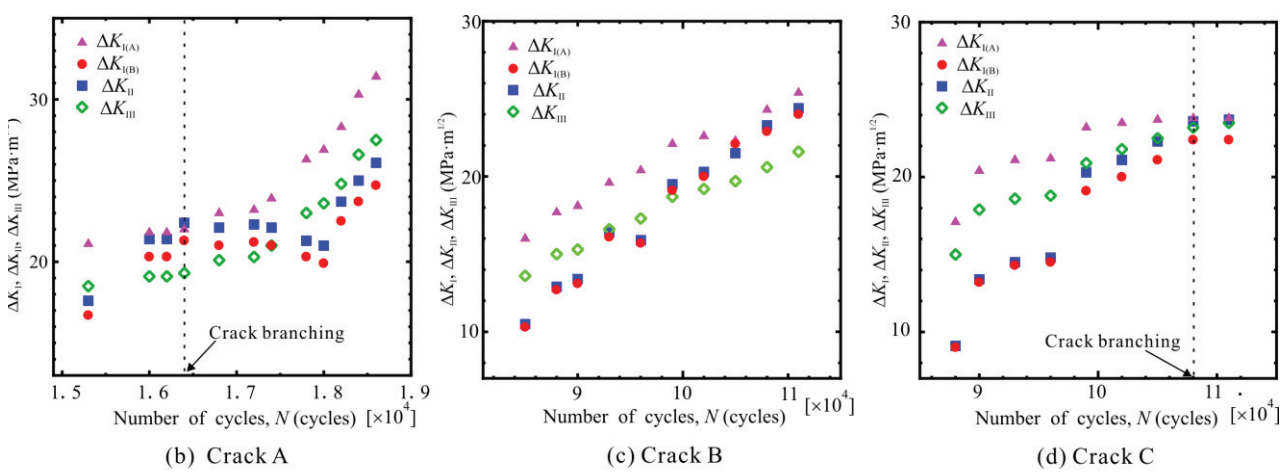

Fig. 10 Change of stress intensity factor range of the crack measured by the CT image, (a): Geometry of crack shape for the calculation of stress intensity factor range.

and $\Delta K_{I(A)}$ and $\Delta K_{I(B)}$ were calculated by using Irwin's equation [10],[11] based on the crack shape projected to the principal plane of stress, as shown in Fig. 10(a). The shear stress distribution was assumed to be constant in the depth direction for simple evaluation of the stress intensity factor. It is found from Fig. 10(b) and (d) that $\Delta K_{I(a)}$ and ΔK_{II} of Crack A and C increased with increasing in the number of cycles, and reached 22~24MPa$\sqrt{m}$ when the crack branching were observed both on and under the surface. For Crack B, the crack branching had not been detected under the surface, and $\Delta K_{I(a)}$ and ΔK_{II} of Crack B were below 22~24MPa$\sqrt{m}$ for the observation period, as shown in Fig. 10(c). From a comparison with the results, it can be concluded that the crack starts to propagate in the opening mode when ΔK_{II} at the crack tip on the surface reaches 22~24MPa$\sqrt{m}$ and ΔK_{I} at the crack tip on the surface is over 22~24MPa$\sqrt{m}$.

4. Conclusions

Imaging to evaluate the torsion fatigue crack propagation property in Ti-6Al-4V were performed by the μCT with the synchrotron radiation of SPring-8. The results obtained are as follows;

(1) A compact torsion fatigue testing machine was developed. It is possible to generates high torque up to 5Nm, and carry out at loading frequency of 20 Hz.

(2) The fatigue crack propagation behavior under reversed torsion was evaluated by the μCT technique. The crack propagation in the depth direction and propagation behavior of branched cracks and kinked cracks could be observed.

(3) The stress intensity factor ranges were calculated by using the three-dimensional crack shape. When the crack starts to propagate in the opening mode, ΔK_{II} at the crack tip on the surface reaches 22~24MPa$\sqrt{m}$ and ΔK_{I} at the crack tip on the surface is over 22~24MPa$\sqrt{m}$.

Acknowledgements

The synchrotron radiation experiments were performed at BL19B2 in SPring-8 with the approval of the Japan Synchrotron Radiation Research Institute (JASRI) under proposal numbers of 2008A1922 and 2009B1895. The authors are grateful for his technical support of Dr. Kentaro Kajiwara (JASRI).

References

[1] Y. Murakami, K. Takahashi and K.Toyama, Mechanism of Crack Path Morphology and Branching from Small Fatigue Cracks under Mixed Loading, Fatigue Fract Engng Mater Struct. Vol. 28, 2005, p. 49-60.

[2] M. Sawada, K. Bannai and M. Sakane, Crack Propagation Direction of Type 304 Stainless Steel in Torsion Low Cycle Fatigue, J. Soc. Mat. Sci., Japan, Vol. 54, No. 6, 2005, p. 615-621.

[3] D. Shiozawa, Y. Nakai, Y. Morikage, H. Tanaka, H. Okado, ,and T. Miyashita, Qantitative Analysis of Inclusions in High-strength Steels by X-ray Computed Tomography Using Ultra-bright Synchrotron Radiation, Transactions of Japanese Society of Mechanical Engineers, Series A, Vol. 72, 2006, p. 1846-1852.

[4] D. Shiozawa, N. Nakai, T. Kurimura, Y. Morikage, H. Tanaka, H. Okado, T. Miyashita, K. Kajiwara, Observation of Cracks in Steels Using Synchrotron Radiation X-ray Micro Tomography, Journal of the Society of Materials Sciencem, Japan, Vol. 56, No. 10, 2007, p. 951-957.

[5] Y. Nakai, D. Shiozawa, Y. Morinaga, T. Kurimura, H. Okado, T. Miyashita, Observation of Inclusions and Defects in Steels by Micro Computed-tomography using Ultrabright Synchrotron Radiation, Fourth Int. Conf. on Very High Cycle Fatigue, J. E. Allison, J. W. Jones, J. M. Larsen, and R. O. Ritchie (Eds.), 2007, p. 67-72.

[6] D. Shiozawa, Y. Nakai, T. Kurimura and K. Kajiwara, Observation of Fretting Fatigue Cracks by Micro Computed Tomography with Synchrotron Radiation, Proc. of 12th International fracture conference, CD-ROM, 2009, OS12.086.

[7] H. Matsunaga, S. Muramoto, N.Shomura and M. Endo, Shear Mode Growth and Threshold of Small Fatigue Cracks in SUJ2 Bearing Steel, Journal of the Society of Materials Science, Japan, Vol. 58, No. 9, 2009, 773-780.

[8] J.P. Campbell, R.O. Ritchie, Mixed-mode, High-cycle Fatigue-crack Growth Thresholds in Ti-6Al-4V, Engineering Fracture Mechanics, 67 2000, p. 229-249.

[9] M.K. Kassir and G.C.Sih, Three-dimensional Stress Distribution Around an Elliptical Crack Under Arbitrary Loadings, Journal of Applied Mechanics, Vol. 33, 1966, p. 601-611.

[10] G.R. Irwin, Crack Extension Force for a Part-through Crack in a Plate, Trans. ASME Ser E: J. Appl. Mech. 29, No.4, 1962, 651-654.

[11] Y. Murakami, Stress Intensity factors Handbook, 2, JSMS, 1987, 696-689.Van der Geer J, Hanraads JAJ, Lupton RA. The art of writing a scientific article. *J Sci Commun* 2000;**163**:51–9.